technische universität
dortmund

Arbeit zur Erlangung des akademischen Grades
Bachelor of Science

Search for single top-quark production in the s-channel with the ATLAS experiment

Alfredo Manente
geboren in Dortmund

2025

Lehrstuhl für Experimentelle Physik IV
Fakultät Physik
Technische Universität Dortmund

Erstgutachter:	PD Dr. Andrea Helen Knue
Zweitgutachter:	Dr. Salvatore La Cagnina
Abgabedatum:	15. Dezember 2025

Kurzfassung

In dieser Arbeit werden Studien zur Messung des Wirkungsquerschnitts für die Erzeugung einzelner Top-Quarks im s-Kanal bei Proton-Proton Kollisionen mit einer Schwerpunktsenergie von $\sqrt{s} = 13\,\text{TeV}$ durchgeführt. Die Daten stammen aus Kollisionsexperimenten des LHC und wurden vom ATLAS Detektor in den Jahren 2015 bis 2018 aufgenommen. Zur Extrahierung des Wirkungsquerschnitts wird ein Profile Likelihood Fit verwendet, wobei als Diskriminante die Ergebnisse eines *Deep Neural Networks*(DNN) fungieren. Die Signal Signatur besteht aus einem geladenen Lepton, entweder Elektron oder Myon, zwei b-tagged Jets und fehlendem transversalen Impuls.

Abstract

The abstract is a short summary of the thesis in English, together with the German summary it has to fit on this page.

Contents

1 Introduction

The Standard Model (SM) of particle physics is the best descriptor for the behaviour of elementary particles and the interactions between them. Despite its major successes many phenomena remain unexplained, like the discovery of the Higgs boson [7, 3] or the top quark [8, 1]. Physics beyond the Standard Model (BSM) is needed to understand the nature of dark matter, neutrino oscillations or the matter-antimatter disbalance. As the heaviest fermion with a mass of about 172.5 GeV [10, 6], the top quark has the strongest coupling to the Higgs field and may act as a potential probe for electroweak symmetry breaking. Therefore in it lies potential in uncovering BSM physics. Its short lifetime of 5×10^{-25} s [12] makes hadronization impossible, which does not enable a direct measurement of the top quark. It almost exclusively decays into a W-boson and a bottom-quark via the weak interaction. In proton-proton (pp) collisions at the Large Hadron Collider (LHC), top-quarks are predominantly produced in top-antitop quark pairs ($t\bar{t}$) via the strong interaction. However, top quarks can be produced singly via the electroweak interaction, with the single-top production in the s- and t-channel, as well as in tW associated production. The s-channel has the smallest cross section of 10.32 pb of all mentioned processes and is dominated heavily by background processes. Unlike the other single top-quark production modes, the s-channel has not yet been measured with a significance over 5σ at the LHC, with the latest ATLAS measurement achieving an observed (expected) significance of 3.3(3.9). [5]. It used a matrix element method (MEM) discriminant in a binned profile likelihood fit to data. Even with its small cross section, the major hindrance in the measurement is the size of the systematic uncertainties. To get a more precise measurement, this thesis will use a more modern approach, with a DNN output as the discriminant for a profile likelihood fit. Simulated data from pp collisions in the LHC at $\sqrt{s} = 13$ TeV measured by the ATLAS detector is used, corresponding to the full Run 2 dataset with a luminosity of 140 fb^{-1}. The structure of this work is as follows: Chapter 2 displays an overview of the SM, the s-channel production mode as well as the dominant backgrounds and the previous measurement. Chapter 3 presents the ATLAS detector. Chapter 4 discusses the simulation, the object definitions and event selections. Chapter 5 describes the main study presented in this thesis. Finally chapter 6 gives a short summary of the results and an outlook to further improvements in the measurement of the single top s-channel.

2 Properties of the Top Quark within the Standard Model

2.1 Overview of the Standard Model

The SM of particle physics is a gauge invariant theory, which describes the fundamental particles and the interactions between them. It was developed throughout the 20th century (citation) by combining the discoveries of quantum mechanics and special relativity into a quantum field theory. Three of the four fundamental forces, electromagnetism, the strong interaction and the weak interaction are characterized by it, only excluding gravity. Whereas electromagnetism and gravity act on infinite ranges, the strong and weak force act on subatomic scales.

The SM divides the fundamental particles into two main categories. First fermions, which constitute all known matter and carry half integer spin. Second bosons, which act out the interactions between fermions and carry a whole integer spin. Further, bosons can be divided into vector bosons, with spin 1 and a scalar boson, the Higgs boson (H) with spin 0. The fermions are comprised of quarks and leptons, where both interact with the electromagnetic (EM) force but only quarks experience the strong force. Neutrinos, which take part in the lepton category, only interact via the weak force. The fundamental particles are further split into three generations in relation to their masses and time of discovery. The first generation is comprised of the electron (e) and the corresponding electron neutrino (ν_{e}) for the lepton part, and the up quark (u) as well as the down quark (d). The second generation leptons include the muon (μ) and the muon neutrino (ν), while the charm quark (c) and the strange quark (s) constitute the second generation quarks. The third generation includes the heaviest fermions, with the tau lepton (τ) and its corresponding tau neutrino (ν_{tau}) on the lepton side and the top quark (t) and bottom quark (b) on the quark side. The electric charge defines the interaction strength with the EM force. All charged leptons posses an electric charge of -1 elementary charge (e). Whereas up-type quarks (u, c, t) carry a charge of $+2/3\,\mathrm{e}$ and down-type quarks (d, s, b) carry a charge of $-1/3\,\mathrm{e}$. For every fermion there exists an antiparticle counterpart with oppsite electric charge and spin. Especially the first generation of fermions constitute to the overwhelming part of matter, where protons and neutrons are build with the u- and d-quarks and electrons as part of atoms.

The force carrying bosons include the photon (γ) for the EM interaction, the $W^{\pm}$ and Z bosons for the weak interaction and eight gluons with different colour for the strong interaction. The photon is mass- and chargeless, with it coupling to every particle possesing an electric charge. The $W^{\pm}$ and Z bosons of the weak interaction carry relatively high mass, which is the reason for its narrow interaction range. The weak force acts on every fermion, where the $W^{\pm}$ bosons couple to the weak isospin and the Z boson couples to the weak hypercharge, a combined value of the electric charge and weak isospin. Gluons, mediating the strong interaction, are massless as well and couple to any particle carrying a colour charge, either quarks or glouns themselves. There are the three base colours red, green and blue with a respective anticolour counterpart. Gluons always carry two colour charges, one base colour and one anticolour, resulting in eight different possible permutations. Quarks carry only one colour charge. Colour confinement states that every stable composite particle has to be colorless, which is the reason for the finite range of the strong interaction. These stable composites are called hadrons and are further split into mesons and baryons. Mesons are colour neutral quark-anitquark pairs. Baryons are colour neutral composites of three quarks. The Higgs Boson, proposed by Peter Higgs in 1964 [**higgs**], was discovered in 2012 in a combined effort of the ATLAS [**atlas_higgs**] and CMS [**cms_higgs**] experiment at the LHC. As a scalar boson it carries spin 0, no electric charge and is the heaviest boson ($m_{\mathrm{H}} = (125.20 \pm 0.11)\,\mathrm{GeV}$ [**higgs_mass**]). It mediates none of the fundamental forces, but by coupling to it fermions and the $W^{\pm}$ and Z boson gain their mass.

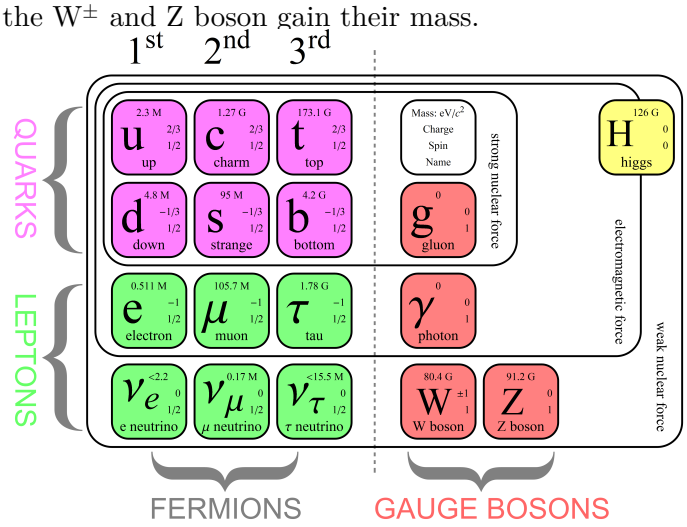

Figure 2.1: The fundamental particles of the Standard Model, showing which forces act on them respectively [15]

2.2 The Top Quark

First postulated by Makoto Kobayashi and Toshihide Maskawa in 1973 [11] and later discovered at Fermilab with the CDF and DØ experiments of the Tevatron collider in 1995 in $p\overline{p}$ collisions [8, 1], the top quark is the last discovered quark in the SM and is the up type quark of the third generation. It carries the heaviest mass of all quarks at $m_{\mathrm{t}} = (172.95 \pm 0.53)\,\mathrm{GeV}$ [6] and posseses a large decay width of $\Gamma_t = 1.42^{+0.19}_{-0.15}\,\mathrm{GeV}$ [4]. This large decay width leads to a short mean life time of $\tau = \hbar/\Gamma_{\mathrm{t}} \approx 5 \times 10^{-25}\,\mathrm{s}$[12]. Unlike other quarks, which hadronize due to colour confinement, the top quark decays before hadronization is possible, due to this short lifetime. The tops properties, like spin information or kinematic properties, are then to be decoded by studying the decay particles, which makes its analysis especially interesting. The top quark decays almost exclusively into a W-boson and a b-quark.

2.3 Single Top Quark Production in the s-Channel

The s-channel is one of the electroweak top-production modes, producing a single top or antitop quark. In the single top-quark s-channel, a top-quark and a bottom anitquark are created from a virtual W-boson, after the annihilation of a quark and antiquark. The s-channel shows a tWb vertex, with the CKM matrix element being almost one. Therefore the s-channel is a strong probe for the electroweak properties of the top quark. At the LHC, the annihilating particles are predominantly valence up quarks (u) and antidown ($\overline{d}$) from the pool of sea quarks in the colliding protons.

(Unterschied zwischen $\overline{u}$ und d als annihilierende Teilchen heraus finden)

The Feynman diagram of the s-channel process at LO in QCD is shown in Figure 2.2a.

(Den folgenden Teil erst bei der simulationen erwähnen)

The parton density function (PDF) is a representation of the probability distrubtion with wich a parton carries a fraction of the momentum of a hadron, denoted by using the *Bjorken x*. $p_i = xp_p$ resembles the momentum fraction the parton i carries from the whole proton momentum p_p. Where a parton is a hadron component, either a quark or gluon. The cross-section $\sigma_{\mathrm{s-chan.}}$ of the single top quark s-channel process, is determined using the factorisation theorem of the QCD. By convolving the PDFs of the parton constituents i and j with the cross section $\sigma_{ij\to t\bar{b}}$ of the respective

sub-process and then summing over all possible sub-processes, the s-channel cross section is determined.

$$\sigma_{\text{s-chan.}} = \sum_{i,j} \int \mathrm{d}x_i f_i(x_i, \mu_{\text{F}}^2) \int \mathrm{d}x_j f_j(x_j, \mu_{\text{F}}^2) \sigma_{ij \to t\bar{b}}(\sqrt{s}, m_t, \mu_{\text{F}}, \mu_{\text{R}}, \alpha_S).$$

The formular takes in, the centre-of-mass energy $\sqrt{s}$ of the process, the top quark mass m_t, the coupling strength of the strong interaction α_S, as well as the factorisation scale μ_{F} and the renormalisation scale μ_{R}, which are set to the energy scale of the process.

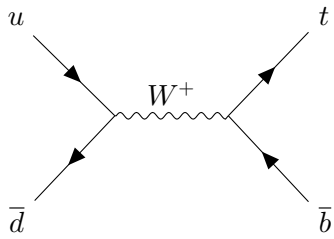

(a) Single top-quark production s-channel

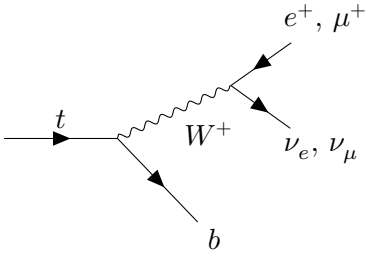

(b) Leptonic decay of the top quark

Figure 2.2: Feynman diagram of the single top quark s-channel production mode (left) and the leptonic decay of the top quark (right).

2.3.1 Top Quark Decay

The top quark decay occurs via the weak interaction, mainly into a b-quark and a W-boson. Furthermore, the W-boson decays either hadronically $^2/_3$ or leptonically $^1/_3$ of the times. The hadronic decay results into two quarks, whereas the leptonic decay results in a charged lepton and its corresponding neutrino. The leptonic decay of the W-boson is shown in Figure 2.2b. As there are different color permutations the quarks can carry, the phase space for the hadronic decay is larger, making it

more likely than the leptonic decay. During the s-channel analysis only leptonic W-boson decays are selected, as the final state from the hadronic decay suffers from multijet background production. If the sum of all transverse momenta of all the outgoing particles, does not add to zero, then a particle has remained undetected and the event has missing transverse momentum $E_{\mathrm{T}}^{\mathrm{miss}}$, as prior to the collision. Events with neutrinos in the final state are therefore expected to have missing transverse momentum.

The searched for signature consist therefore of a charged lepton from the leptonic W-boson decay, missing transverse momentum $E_{\mathrm{T}}^{\mathrm{miss}}$ from the undetectable neutrino, and two b quarks, one produced from the s-channel process itself and one from the b-quark of the top-quark decay. τ leptons have a short lifetime and can thus not be directly detected, but first and second generation leptons from the τ decay can be observed. Because of that lepton signature is narrowed down to either an electron or muon.

2.3.2 Background Processes

There are physics processes with similar signatures in the detector as the signal process discussed above. Differentiating these processes from the process of interest is a major task in any analysis. These so-called background processes consist predominantly of $t\bar{t}$ production and W+jets production for the single top s-channel analysis. In the LHC collisions, $t\bar{t}$ production occurs mostly through gluon-gluon fusion, but with less probability can also happen through quark-pair-annihilation. With a theoretical cross-section of $\sigma_{t\bar{t}}^{\mathrm{Theo.}} = 832^{+20}_{-29}\,\mathrm{pb}$[**ttbar_cross**], it exceeds every other top quark production mode. The other single top quark production modes can be mistaken for signal as well, but to a lesser degree, since their cross sections are noticeably smaller than $t\bar{t}$ with $\sigma_{t-\mathrm{chan.}}^{\mathrm{Theo.}} = 216.99^{+9.04}_{-7.71}\,\mathrm{pb}$ [**tchan_xsec**] and $\sigma_{tW-\mathrm{Prod.}}^{\mathrm{Theo.}} = (71.7 \pm 3.8)\,\mathrm{pb}$ [**tw_xsec**]. Other minor backgrounds stem from multijet background processes, Z+jets or diboson(WW,WZ,ZZ) production. Figure 2.3 shows the LO Feynman diagrams for $t\bar{t}$ production via gluon-gluon fusion, and the other two single top-quark production modes.

Not only does the $t\bar{t}$-production mode hold a large cross-section, but the fact that it produces real top-quark decays makes it a difficult background. The two W-bosons, resulting from the t-quark and $\bar{t}$-quark decay, again can decay leptonically or hadronically. If both W-bosons decay leptonically, the dileptonic final state, can mimic the signal signature if one of the leptons stays undetected. For the semileptonic decay, where one W-boson decays leptonically and one hadronically, the final state signature can emulate the signal if only two b jets get detected. The fully hadronic decay is very unlikely to be mistaken for the signal. Likewise the

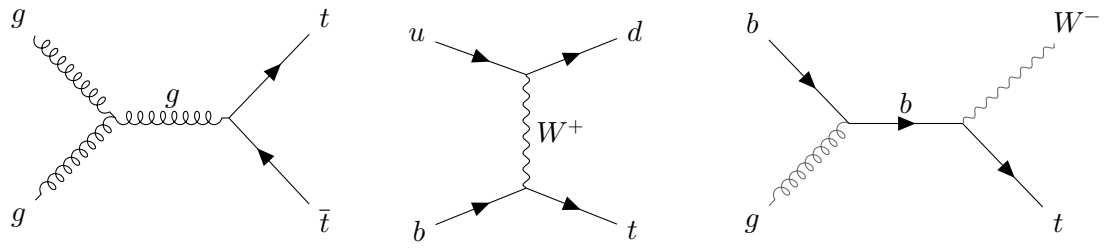

(a) $t\bar{t}$ production through gluon gluon fusion.

(b) Single top t-channel.

(c) Associated tW production.

Figure 2.3: Feynman diagrams at LO for the major background processes in the analysis of the single top quark s-channel production mode.

single top-quark production mode in the t-channel and the associated tW production also show real top quark decays in their signatures. For the t-channel the final state reproduces the signal signature if a b jet or misidentified lighter quark jet gets associated with the event. In the associated tW-production, the b-quark turns into a t-quark by emitting a W-boson. If this W-boson decays hadronically and produces a b jet or a jet that gets misidentified, the final state signature is the same as the signal signature. If the W-boson decays leptonically and two b jets or misidentified jets get associated with the event, the W+jets background also mimics the signal. In the case of multijet background, leptons from heavy flavor decays, electrons from photon conversion or jets misidentified as leptons paired with two b jets or misidentified jets lead to the signal signature.

2.3.3 Previous Measurements

- Beschreibe welche Unsicherheiten genau die vorherige Messung verschlechtert

In Figure 2.4 previous measurements of the three different single top-quark production modes at different center of mass energies $\sqrt{s}$ are shown, taken at the ATLAS and CMS experiments at the LHC with data from pp-collisions.

The most recent measurement of the s-channel was done by ATLAS with a center of mass energy of $\sqrt{s} = 13\,\text{TeV}$, with data collected between the years 2015 and 2018, corresponding to the Run 2 dataset at an integrated luminosity of $140\,\text{fb}^{-1}$. The cross section of the measured s-channel resulted in $\sigma_{\text{s-chan}} = 8.2 \pm 0.6(\text{stat.})^{+3.4}_{-2.8}(\text{syst.})\text{pb}$, in comparison to the theoretical estimate of $\sigma^{\text{theo.}}_{\text{s-chan}} = 10.32^{+0.40}_{-0.36}\,\text{pb}$. This is equivalent with an observed (expected) signal significance over the background only hypothesis of $3.3(3.9)\sigma$. The analysis strategy consisted of a preselection and then a split into one signal region and three validation regions, for better modelling of

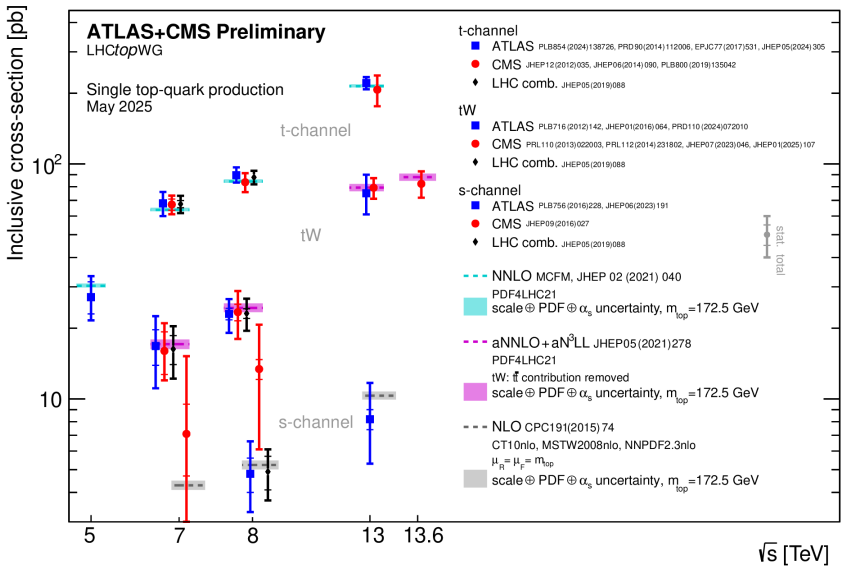

Figure 2.4: Chart of all measurements taken of the three different sinlge top production modes at the ATLAS and CMS experiments [**prev_measure**]

the background processes. To extract the signal strength from the events, a profile likelihood fit was done, with a matrix element method (MEM) discriminant. The limiting factors of the previous measurement where noticeably the systematic uncertainties, where $t\bar{t}$ modelling and signal modelling uncertainties, as well as detector modelling uncertainties, had the biggest impact (Irgendwie muss ich das ja noch zeigen? Wie soll ich da mit der Systematics Tabelle aus dem Paper umgehen?).

3 The ATLAS Detector

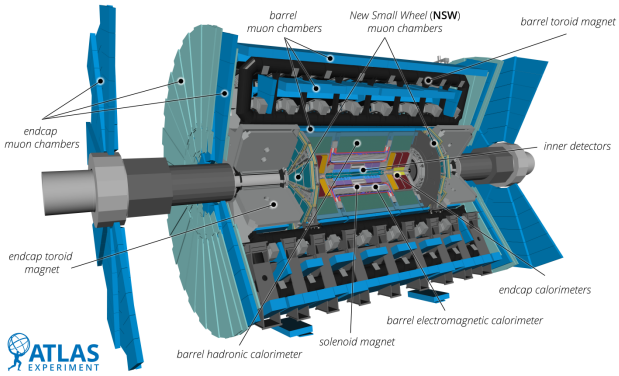

Figure 3.1: Schematic overview of the ATLAS Detector and all its subsystems [2]

As a general purpose detector, the ATLAS detector covers a solid angle range of 4 π. The full angular coverage in the beams symmetry plane is granted through its cylindrical design, with a central barrel and two endcaps. It consists of three main subsystems, which are the *Inner Detector* (ID), the *Calorimeter System* and the *Muon Spectrometer* (MS). With the help of a 2 T solenoid magnet, the trajectory of charged particles are bent using the Lorentz force and then reconstructed inside the ID. The calorimeter system consists of an Electromagnetic Calorimeter (ECAL) and Hadronic Calorimeter (HCAL). Inside the ECAL the incoming electrons and photons trigger showers, which ionize parts of the calorimeter and results in energy and direction measurements. Similarly, the HCAL absorbs hadronic jets and triggers hadronic showers, leading to light emissions in the scintillator tubes of the HCAL, from which energy and direction of the jets are determined. As minimal ionizing particles, muons pass all the previously mentioned subsystems and can only be detected in the MS. Here the toroidal magnets in the endcap and barrel parts of the detector bend their tracks and helps in trajectory and charge measurements.

Cartesian coordinates within the LHC are defined as follows: The z-axis is aligned with the beam pipe, the x-axis points to the center of the LHC and the y-axis points upwards to the beam plane. To introduce spherical coordinates, ϕ is used to describe the angle between the y- and x-axis, while θ describes the angle between the y- and z-axis. Lorentz invariance can then be achieved by introducing the pseudorapidity

$\eta = -\ln(\tan\frac{\theta}{2})$. Particle distances within the detector are then defined by the value $\Delta R = \sqrt{\Delta\eta^2 + \Delta\phi^2}$. Transverse momentum is calculated within the cartesian coordinates with $p_{\mathrm{T}} = \sqrt{p_x^2 + p_y^2}$.

4 Object Definition and Event Selection

4.1 Monte Carlo Samples

In order to study processes in particle physics, signal processes have to be seperated from background processes. Instead of only using recorded data, simulations are done, to better compare these processes with their SM predicitons, via varying assumptions and parameters. In this thesis the single top-quark s-channel production mode is to be examined, with the major backgrounds being $t\bar{t}$-production, single top-quark production in the t-channel, associated tW-production, W+jets and Z+jets production. As multijet background is estimated via fits to data, it is dropped out of consideration. Monte Carlo (MC) simulators are used to reproduce particle events using a Markow Chain process. At LO and NLO, hard scattering events can be calculated using pertubation theory, by calculating the relevant matrix elements (ME). Whereas parton showers (PS) and hadronization due to the strong interaction have to be calculated, utilizing phenomenological models to incorporate the effects of confinement and asymptotic freedom present in QCD. These models use different hadronization models and free parameter, which are tuned using recorded data. As a general purpose MC simulator Sherpa can calculate the hard scattering ME, as well as parton showers and hadronisation. Powheg box v2 can generate hard scattering events up to NLO. Pythia 8 models parton shower and hadronisation via the *Lund String model*, typically making use of the *A14* tune. Herwig 7 calculates parton showers and hadronisation via the *heavy cluster model*. Finally, Evtgen simulates the decay of heavy-flavour hadrons, especially b and c hadrons. During all simulations a top-quark mass of 172.5 GeV is utilized.

For the nominal single top-quark and antitop-quark s-channel samples, Powheg simulations combined with Pythia are used under the *A14* tune. Heavy-flavour decays are further calculated by Evtgen.

The t-channel single top-quark and anti-quark processes similarly make use Powheg and Pythia. The leptonic decay of the W-boson from the top-quark decay is enforced and a Breit-Wigner propagator scheme with a fixed top-quark width of 50 GeV is used.

Associated tW production samples are generated with POWHEG interfaced with PYTHIA, while further making use of the diagram removal scheme (citation) to handle interference with $t\bar{t}$ production at NLO. The NNPDF3.0NLO PDF set is used in HERWIG for these samples.

The $t\bar{t}$ production is both simulated with the full-sim and fast-sim detector model, while utilizing the POWHEG generator at NLO with the NNPDF3.0NLO PDF set, combined with PYTHIA. The h_{damp} parameter, which regulates the first gluon emission beyond the Born configuration (Was ist das?), is set to $1.5 \cdot m_{\text{top}} \simeq 258.75\,\text{GeV}$.

For the W+jets samples the SHERPA 2.2.11 version is used, instead of SHERPA 2.2.14. Here SHERPA calculates the matrix elements at NLO accuracy for up to two partons and at LO accuracy for up to five partons, which is combined with parton shower models.

The Drell-Yan production modes of $Z \to ee$, $Z \to \mu\mu$, $Z \to \tau\tau$ are simulated with SHERPA 2.2.11 for the light leptons. For tau decay SHERPA 2.2.14 with the NNPDF3.0NNLO PDF set is utilized. Samples inside different invariant-mass regions, involving a low-mass interval of ($10 < m_{ll} < 40\,\text{GeV}$), is used to improve description of dilepton spectra.

4.2 Object Definition

The signal signature consist of different objects of significance: leptons, either electrons or muons, and their corresponding neutrinos, as well as hadron jets, especially important b-tagged jets. To reconstruct these objects from the detector response a framework for the respective object defintions is to be used.

Electrons are reconstructed from particle tracks in the ID and energy deposits in the ECAL. A measured $p_{\text{T}} > 10\,\text{GeV}$ and $|\eta_{\text{cluster}}| < 2.47$, while deposits in the barrel-end cap transition region $1.36 < |\eta_{\text{cluster}}| < 1.52$ are discarded, are necessary, as well as passing the TightLH and isolation working point, for an electron to be identified as such. Muons require at least a $p_{\text{T}} > 10\,\text{GeV}$ and $|\eta| < 2.5$, while passing the medium quality definition and tight isolation working point. Jets are reconstructed with the anti-k_t algorithm with a radius parameter of $\Delta R = 0.4$. The GN2v01 algorithm, determines if a jet is to be determined as b-tagged.

4.3 Event Selection

With the expected signal signature in mind, a framework for the event selection is used. For single top quark production in the s-channel, a charged lepton, either electron or muon, missing transverse momentum $E_{\mathrm{T}}^{\mathrm{miss}}$ from the undetected neutrino, and two b-tagged jets are expected. A preselection in the ntuple production inside TopCPToolkit is utilized. Only events with at least two b-tagged jets with $p_{\mathrm{T}} > 20\,\mathrm{GeV}$, of which at least one must fullfill the 85% working point requirements, and exatly one isolated lepton with $p_{\mathrm{T}} > 28\,\mathrm{GeV}$, survive. The precise event selection is then achieved inside FastFrames, a software tool to further process ntuples and gather histograms from. For this analysis a single signal region (SR) is defined, without any other validation regions. Events inside the signal region encompass two central jets, each in a $|\eta| < 2.5$ range and fulfilling the 77% b-tagging working point. Further transverse momentum requirements are used, where the leading jet has to satisfy $p_{\mathrm{T}} > 40\,\mathrm{GeV}$, while the subleading jet requires $p_{\mathrm{T}} > 30\,\mathrm{GeV}$. Exactly one isolated lepton, either an electron or muon, with $p_{\mathrm{T}} > 30\,\mathrm{GeV}$ has to be included. An additional lepton veto discards all events with an extra lepton with $p_{\mathrm{T}} < 30\,\mathrm{GeV}$. The missing transverse momentum of the undetected neutrino in an event has to fulfill $E_{\mathrm{T}}^{\mathrm{miss}} > 35\,\mathrm{GeV}$, while the reconstructed transverse mass of the W-boson,

$$m_T^W = \sqrt{2p_{\mathrm{T}}^l E_{\mathrm{T}}^{\mathrm{miss}}(1 - \cos \Delta\phi(l, E_{\mathrm{T}}^{\mathrm{miss}}))}$$

is required to be $m_T^W > 30\,\mathrm{GeV}$. Another additional jet veto is used, where events with additional jets carrying $p_{\mathrm{T}} > 30\,\mathrm{GeV}$ or additional jets in the forward region ($|\eta| > 2.5$) are rejected. The SR definition with all the event selection cuts used in this analysis is shown in Table 4.1.

Table 4.1: Definition of the event selection for the Signal Region used in this analysis.

	SR
n(e, μ)	== 1 with $p_{\mathrm{T}} > 30\,\mathrm{GeV}$
n(jets)	== 2, in $\lvert\eta\rvert < 2.5$
n($b-tags$)	== 2, @77%, in $\lvert\eta\rvert < 2.5$
Leading jet p_{T}	$> 40\,\mathrm{GeV}$, in $\lvert\eta\rvert < 2.5$
Subleading jet p_{T}	$> 30\,\mathrm{GeV}$, in $\lvert\eta\rvert < 2.5$
Missing transverse energy ($E_{\mathrm{T}}^{\mathrm{miss}}$)	$> 35\,\mathrm{GeV}$
Transverse W boson mass	$> 30\,\mathrm{GeV}$
Additional jets (low p_{T}) veto	No jets with $p_{\mathrm{T}} < 30\,\mathrm{GeV}$
Forward jets veto	No jets with $\lvert\eta\rvert > 2.5$
Additional leptons veto	No extra leptons with $p_{\mathrm{T}} < 30\,\mathrm{GeV}$

s-channel	4139.990 ± 850.839
single top tchan	9334.36 ± 1853.71
single top tW	2619.050 ± 612.957
Z+jets	1654.390 ± 882.368
W+jets	$15\,159.50 \pm 7858.56$
ttbar	$75\,216.7 \pm 18\,753.3$
Total	$108\,124.0 \pm 24\,971.1$

Table 4.2: Yields of the analysis

5 Analysis and Results

5.1 Analysis Strategy

Throughout this analysis, steps are taken to determine the signal strength $\mu_{\text{s-chan.}} = \sigma^{\text{measured}}_{\text{s-chan.}} / \sigma^{\text{theory}}_{\text{s-chan.}}$ of the single top quark s-channel process. This is done via a binned likelihood fit, where a *Deep Neural Network* (DNN) output is used as discriminant value, to descern signal events from background events. Only one signal region, pulled from the event selection in Table 4.1, is defined in this thesis. As systematic uncertainties are the limiting factors in the search for the single top quark s-channel process, the systematics with the biggest impact are further inspected and discussed.

5.2 DNN Model

Especially in studying the single top quark s-channel process, a modern machine learning approach is sensible as the small signal to background ratio ($S/B 3.4\%$) [14] makes traditional methods difficult. Therefore a DNN output will be used as the discriminant for a binned likelihood fit. The applied DNN was designed by Niklas Düser as part of his Master's Thesis at the *Technische Universität Dortmund* [9] and makes use of several high-level kinematic variables to descern signal events from background events. For every single particle that gets reconstructed, the kinematic variables $p_{\text{T}}, \eta, \varphi$ and the invariant mass m get included as features for the DNN model. Whereas for particle pairs their pseudorapidity difference $\Delta\eta$ and the difference in azimuthal angle $\Delta\varphi$ between them is incorporated as feature. From the detector measurements of the final state particles, every other particle can be retraced up to the virtal W-boson. First, the final state lepton and corresponding neutrino are reproduced. The neutrino cannot be measured directly via the detector but is inferred via studying the missing transverse momentum $E^{\text{miss}}_{\text{T}}$ of the event and further implying the longitudinal impulse of the neutrino, from the condition that the leptons and the neutrinos momentum squared must equal the invariant mass of the decaying W_{Decay}-boson. With the lepton and neutrino reconstructed, the W_{Decay}-boson of the top quark decay can be solved for. The leading b-tagged jet, of the top quark decay gets measured directly by the detector. With information

about the leading b-jet and the W_{Decay}-boson, the top quark can be reconstructed. From detector measurements, the subleading b-jet from the s-channel process itself gets assessed, and with the reconstructed top quark, the last possible step is to reconstruct the virtual $W_{\text{Prod.}}$-boson. Further the transverse mass of the W_{Decay}-boson defined as $m_{\text{T}}^{\text{W}} = \sqrt{2p_{\text{T}}^{l} E_{\text{T}}^{\text{miss}}(1 - \cos \Delta\varphi)}$, with p_{T}^{l} the transverse momentum of the lepton decay product and $\Delta\varphi$ the angle between lepton and neutrino, is included as feature. As well as the transverse mass of the top quark, defined as $m_{\text{T}}^{\text{top}} = \sqrt{E_{\text{T,sum.}}^2 - p_{\text{T,sum.}}^2}$, with the sums of the transverse energies and transverse momenta of the top quarks decay particles, being the lepton, neutrino and b-quark. The scalar sum of the transverse energies of all final-state paricles is called H_{T}, whereas $H_{\text{T,had.}}$ and $H_{\text{T,lep}}$ sum only over the transverse energies of the final state hadrons or leptons respectively. Another set of event shape variables are inferred through the momentum tensor, that encodes the high-levels momentum distributions of the reconstructed objects. Its elements are derived by the formular

$$M_{ij} = \frac{\sum_{k=1}^{N} p_{k,i} p_{k,j}}{\sum_{k=1}^{N} p_k^2}, \; i, j \in x, y, z$$

by summing over all final-state particles, where $p_{k,i}$ denotes the i-th component of the k-th final state particle. Through the sorted eigenvalues of the momentum tensor $\lambda_0 > \lambda_1 > \lambda_2$ further event variables are constructed:

$$\begin{aligned} &\text{Aplanarity}: && \mathcal{A} = \frac{3\lambda_2}{2}, \\ &\text{Planarity}: && \mathcal{P} = \frac{3(\lambda_2 + \lambda_1)}{2}, \\ &\text{Spericity}: && \mathcal{S} = \lambda_1 - \lambda_2. \end{aligned}$$

The model was trained on both fullsim and fastsim datasets, as well as including single top quark s-channel samples with varying top quark masses for increased statistics. Angular variables are cosine transformed to avoid discontinuities at $\pm\pi$ and variables carrying long tails are log-transformed to compress their dynamic range. All variables are transformed into standardised units, to avoid distortion of variable importance due to their absolute values. Data is split into even and odd samples, only in respect to their event number without taking any other variable feature into consideration. The DNN model outputs a value between 0 and 1, where 1 marks an event as totally corresponding to the signal and 0 marks the event

as background. The DNNs output is shown in the form of the separation plot in Figure 5.1a and the combined DNN output histograms of each respective process shown in Figure 5.1b. The event yields given out from the DNN are shown in **??**.

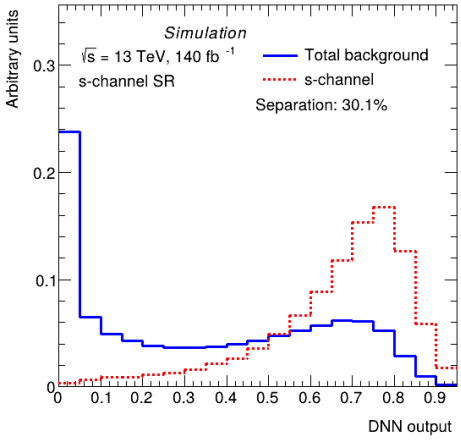

(a) The separation plot shows the output score of the DNN on the x-axis for the s-channel signal histogram and the sum of the background histograms. Both histograms are normalised. A separation of 30.1% is achieved, displayed by the observably separated peaks with yet significant overlap of both distributions.

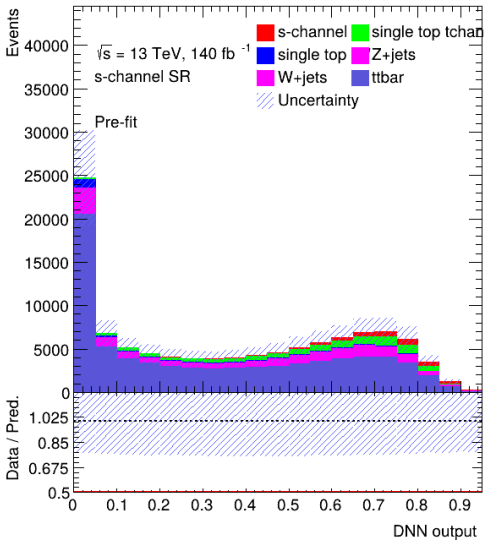

(b) The combined DNN output for every process of interest in this analysis. Histograms are stacked, where the signal yield is displayed in red on the top of the stack.

Figure 5.1: The DNNs output is shown with a separation plot and the combined DNN output for the different processes

5.3 Statistical Method

With the neural network output x as the discriminant, the expected number of events in the i-th bin $\lambda_i(\mu, \theta) = \mu \cdot s_i(\theta) + b_i(\theta)$ is used to incorporate the signal strength. Here $s_i(\theta)$ and $b_i(\theta)$ signify the expected signal and background contributions respectively, which are obtained by processing the simulated signal and background events through the trained DNN model and evaluating the corresponding output score x. The parameter μ represents the signal strength and scales the overall signal contribution uniformly across all bins, while the nuisance parameters (NPs) θ encode the effect of systematic uncertainties on both the normalization and the shape of the signal and background distributions. To determine the cross-section, a *binned profile likelihood fit* is performed with the HistFactory tool (citation). This framework is

used to extract the signal strength parameter μ together with the NPs describing systematic uncertainties by maximizing the likelihood function. This determines the parameter values that best describe the data assuming the presence of the single top quark s-channel signal. The likelihood function states the probability by which an outcome happens with respect to a set of given model parameters. Since analyses in High Energy Physics involve large event samples, the data are represented in histograms, where events are grouped into bins rather than treated individually. The binning of data also introduces Poisson probabilities into the likelihood as can be seen in the following equation.

$$\mathcal{L}(\mu, \theta) = \prod_{i=1}^{N_{\text{bins}}} \text{Pois}(n_i|\lambda_i(\mu, \theta)) \cdot \prod_{j=1}^{N_{\text{NP}}} \pi_j(\theta_j).$$

The binned likelihood function multiplies the Poisson probabilities $\text{Pois}(n|\lambda)$ in each bin, which state the probability of observing n events under the expectation λ

$$\text{Pois}(n|\lambda) = \frac{\lambda^n e^{-\lambda}}{n!},$$

multiplied with the product of all constraint terms $\pi_j(\theta_j)$ for each NP j. A NP of $\theta_j = 0$ conforms to the nominal prediction made by the simulation, while $\theta_j = \pm 1$ represents a variation of one standard deviation $\pm\sigma$. For most systematic uncertainties, the constraint terms are modelled as Gaussian distributions centered at the nominal value θ_j^0 with a width corresponding to the estimated uncertainty $\sigma_{\theta_j^0}$. The one standard deviation variations are provided in the form of up and down shifted histograms. Statistical uncertainties arising from the limited number of simulated events are included as dedicated NPs γ_i for each respective bin i, which are modelled as Poisson-constrained parameters with a nominal value of 1.

By maximizing the likelihood function via variaton of the parameters μ and θ_j, their final values are determined by $\hat{\mu}, \hat{\theta} = \underset{\mu,\theta}{\text{argmax}}\, \mathcal{L}(\mu, \theta)$. In practice, the negative logarithm of the likelihood function $-\ln \mathcal{L}$ is minimized, as the maximum is unaffected by taking the logarithm and the multiplications are transformed into sums. Summing over the logarithms and minimizing is computationally more robust. The negative log-likelihood (NLL) function is minimized with MINUIT (citation). μ and all NPs can vary while fitting. μ is free-floating, while the NPs are penalized based on their respective uncertainties. If after the fit the uncertainty of a NP is smaller then the provided uncertainty $\sigma_{\theta_j^0}$, the fit achieved a constraint on the respective systematic uncertainty.

To assess the expected sensitivity of the analysis and study the impact of systematic uncertainties in the absence of statistical fluctuations, an *Asimov fit* is performed. The *Asimov dataset* is constructed by replacing the observed event counts in each bin with their expected values under the nominal signal-plus-background hypothesis. The Asimov fit provides the expected best-fit values and uncertainties of the signal strength and nuisance parameters, assuming perfect agreement between data and the model.

5.4 Systematic Uncertainties

The systematic uncertainties are categorized into modelling uncertainties of the single top quark s-channel signal process, background modelling uncertainties with a particular focus on the $t\bar{t}$ process, and detector modelling uncertainties.

Modelling uncertainties arise from different theoretical descriptions of the hard-scattering process and its subsequent evolution, including variations in ME calculations, PS modelling, hadronization, and the choice of generator-specific parameters. For the single top quark s-channel signal process, additional MC samples were produced by varying the p_{T}^{hard} parameter to 1, compared to the nominal value of 0. The p_{T}^{hard} variable determines how the event hardness calculated by POWHEG is passed to PYTHIA to regulate the parton shower. By default, the hardness scale *SCALUP* provided by POWHEG is used directly. When setting $p_{\mathrm{T}}^{hard} = 1$, the event hardness is instead defined by the transverse momentum of the hardest POWHEG emission [16]. This variation probes uncertainties related to the matching between the NLO matrix element and the parton shower. In addition, samples interfacing POWHEG with HERWIG were generated to assess uncertainties originating from different parton shower and hadronization models. Similar modelling variations were applied to the $t\bar{t}$ background process. Further $t\bar{t}$ samples were produced with $p_{\mathrm{T}}^{hard} = 1$, and with the *h_damp* parameter increased from $1.5 \cdot m_{top}$ to $3 \cdot m_{top}$, allowing the study of uncertainties related to the modelling of high-p_T radiation in the hardest emissions.

In addition to ME and PS modelling uncertainties, background processes are subject to uncertainties in their theoretical cross-section predictions, which affect their normalisation. A cross-section uncertainty of 6% is assigned to the $t\bar{t}$ background and to the single top quark production modes. For the W+jets and Z+jets background processes, a conservative uncertainty of 50% is assumed.

Detector modelling uncertainties include both one-sided and two-sided systematic variations. Two-sided systematics are provided with independent up and down variations, while one-sided systematics are symmetrised with respect to the nominal

distribution. The latter include uncertainties on the missing transverse momentum $E_{\mathrm{T}}^{\mathrm{miss}}$, parametrising the resolution of the Track Soft Term (TST) in directions parallel and perpendicular to the hard-scatter axis. The integrated luminosity uncertainty is taken to be 0.83% [**lumi_unc**]. Jet-related uncertainties include jet energy resolution (JER), jet vertex tagger (JVT), and jet energy scale (JES) uncertainties. The JER uncertainty is represented by 15 NPs, while two efficiency-related nuisance parameters are used for JVT. The JES uncertainty accounts for effects related to jet flavour composition, flavour response, b-jet energy scale, pile-up, punch-through, and jet η intercalibration, as well as various pre-recommendations, and is encoded using 32 nuisance parameters. Flavour tagging uncertainties are modelled using 55 nuisance parameters for b-tagging, 33 for c-tagging, and 42 for light-flavour jet tagging. In addition, four nuisance parameters per flavour are included to describe uncertainties arising from the extrapolation of the jet calibration to the high transverse momentum regime, where direct experimental constraints are limited. Uncertainties related to the modelling of electrons and muons are also considered. For electrons, six nuisance parameters are included, covering trigger efficiencies as well as energy scale and resolution effects for electrons and photons. For muons, 16 nuisance parameters are used to describe momentum scale and resolution uncertainties, as well as trigger-related effects. The uncertainty associated with pile-up reweighting is represented by a single nuisance parameter.

Additional theoretical uncertainties affecting both the single top quark s-channel signal and the $t\bar{t}$ background arise from variations of the renormalisation and factorisation scales, as well as from initial- and final-state radiation modelling.

In order to be less dependent on statistical fluctuations, the systematics distributions are smoothed. For uncertainties containing an up and down variation, two-sided symmetrization is applied. The up and down variation for each respective bin i consists therefore of the mean of both, given by $\pm\frac{n_i^{\mathrm{up}}-n_i^{\mathrm{down}}}{2}$. Uncertainties with only an up or down variation undergo one-sided symmetrisation, in which the the existing variation is mirrored for the missing counterpart.

5.5 Results

After fitting the NLL onto the Asimov Dataset, the expected signal strength is found to be $\mu_{\mathrm{s-chan.}} = 1^{+0.25}_{-0.20}$. The DNNs output is therefore still consistent with the SM prediction, even after incorporating several more systematic uncertainties into this analysis, as were considered in Niklas Düser's work. From the fit the NPs influences on the signal strength are now accessible. The ranking plot sorts the NPs, with the most influential NP shown on the top of the plot, based on their impact on the

signal strength. Their respective impacts are calculated using the *covariance matrix method* [13]. Here the impact $I = \sigma^a_{\text{total}} C_{a,n} \sigma^n$ is determined with the correlation $C_{a,n}$ between the POI a and the NP n, the total uncertainty σ^a_{total} of the NP and the uncertainty σ^n of the POI. The ranking therefore reflects the sensitivity of the analysis to variations of individual nuisance parameters and provides insight into the dominant sources of systematic uncertainty. The ranking plot for this analysis is displayed in Figure 5.2

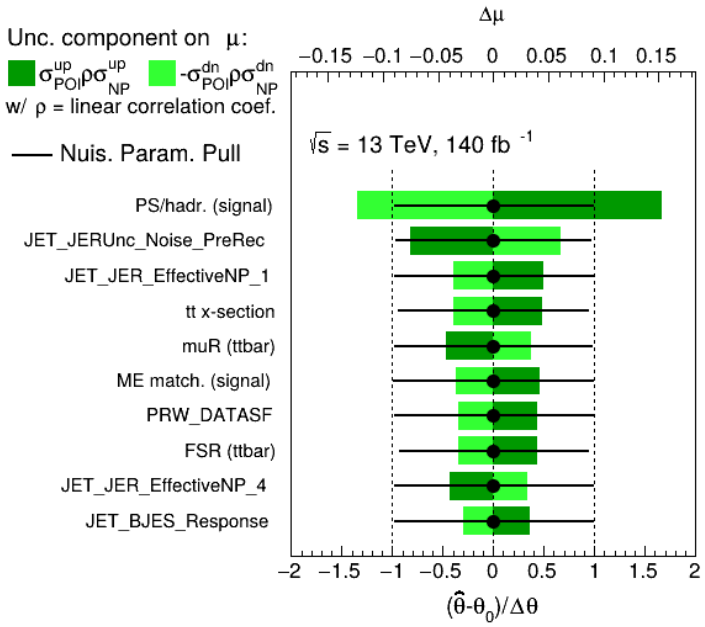

Figure 5.2: The ranking plot sorts the NPs from top to bottom regarding their impact on the signal strength.

The ranking plot reveals that the dominant uncertainty originates from the PS and hadronization modelling of the single top quark s-channel signal process. This is expected, as the hadronic signature of the signal consists only of two b-tagged jets, whose relative kinematics are strongly influenced by the modelling of hard emissions and subsequent showering. The leading and subleading jet transverse momenta are the most impactful input features of the DNN, as seen in section 5.2. This explains the strong sensitivity to PS and hadronisation uncertainties, as these directly affect the jet kinematics exploited by the classifier. On detector level, jet energy resolution uncertainties, in particular the noise pre-recommendation uncertainty and the effective NP 1 uncertainty, have a sizable impact. These uncertainties affect the reconstructed jet momenta and therefore propagate directly to high-level kinematic variables used by the DNN. Uncertainties related to the

modelling of the $t\bar{t}$ background, including the theoretical prior on the $t\bar{t}$ cross-section and the renormalisation scale uncertainty μ_{R}, also show a significant impact. As $t\bar{t}$ constitutes the dominant background process and the signal-to-background ratio of the single top s-channel is small, the analysis is particularly sensitive to variations in the $t\bar{t}$ kinematic description. In particular, variations of the renormalisation scale affect the amount of QCD radiation in the $t\bar{t}$ process, leading to altered jet multiplicities and kinematic distributions, which in turn influence the DNN output. In addition to parton shower and hadronisation uncertainties, the ME matching uncertainty exhibits a strong impact on the extracted signal strength. The ME matching procedure governs the transition between hard emissions described by the fixed-order matrix element and soft or collinear radiation modelled by the PS. For the single top quark s-channel process, which is characterised by a very simple hadronic final state consisting of only two b-tagged jets, the modelling of additional radiation plays a particularly important role. Variations in the ME matching scheme affect the jet multiplicity as well as the transverse momentum and angular correlations of the b-jets. Since the DNN relies strongly on jet-related high-level kinematic variables, these modelling differences propagate directly to the classifier output, leading to a sizeable shape effect. Moreover, the ME matching uncertainty cannot be efficiently constrained by the fit, as it does not primarily affect the overall normalisation but rather the kinematic structure of the signal events. Pile-up refers to additional pp interactions occurring in the same or neighbouring bunch crossings as the hard-scatter event. These interactions introduce extra tracks and energy deposits in the detector, which can bias the reconstruction of jets, missing transverse momentum and other event-level observables. Uncertainties related to pile-up reweighting therefore affect jet multiplicities, jet energies and several high-level kinematic variables, and consequently propagate to the DNN classification. Final State Radiation (FSR) uncertainties of the $t\bar{t}$ background process similarly influence hadronic signatures from the major background source. The remaining JER and JES uncertainties also effect the jet reconstruction on the detector level. Overall, the dominant uncertainties are those affecting the kinematic properties of jets and the modelling of QCD radiation, highlighting the strong interplay between the DNN-based event classification and the theoretical and detector-level description of jet-related observables. Ratio plots of the uncertainties discussed in detail are shown in Figure 5.3. These plots show the relative variation of a given observable under the up- and down-variations of a NP with respect to the nominal prediction.

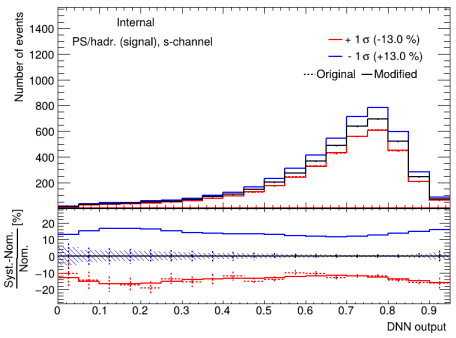

(a) PS and hadronization modelling uncertainty for the signal process.

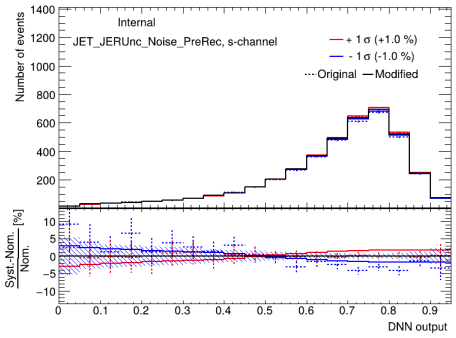

(b) The jet energy resolution noise prerecommendation uncertainty for the signal process.

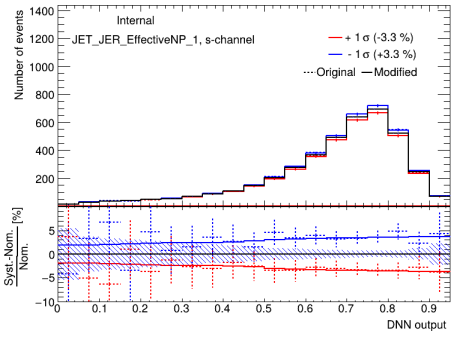

(c) The jet energy resolution effective NP 1 uncertainty for the signal process.

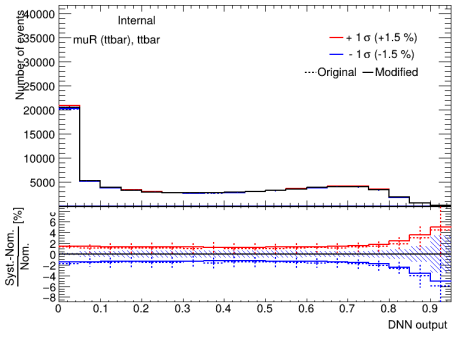

(d) Uncertainty for the renormalisation factor μ_{R} for the $t\bar{t}$ background process.

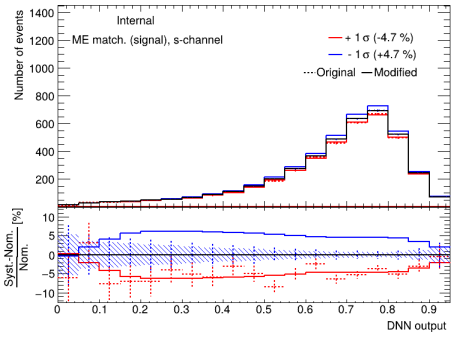

(e) ME matching uncertainty for the signal process.

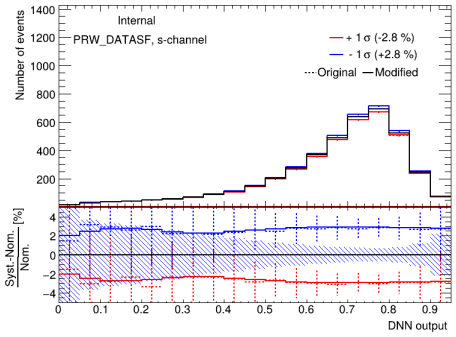

(f) The pile-up reweighting uncertainty for the signal process.

Figure 5.3: Ratio plots for the six uncertainties with the largest impact on the signal strength in this analysis. The upper pad of each plot displays the nominal distribution together with the up- and down-variations, while the lower pad shows the ratio.

The overall impact of systematic uncertainties is reduced in this analysis compared to the previous measurement. This improvement is illustrated in Table 5.1, which shows the percentage impact of the systematic uncertainties grouped by categories. For the comparison of the impact of systematic uncertainties between analyses, the category-wise impacts were determined. All nuisance parameters within a given category were fixed and then fitted, and the resulting change in the signal strength was compared to the nominal full fit.

The reduction of the uncertainties can be attributed to the DNN's ability to exploit a large set of high-level kinematic features and to capture non-linear correlations between them. In contrast, the MEM is limited to a smaller set of observables and simplified correlations, which makes it more sensitive to individual variations in the input distributions. In addition, several systematic uncertainties have been refined since the previous measurement. The ME matching uncertainty for the respective MC samples has been updated, the JER uncertainty now includes a larger set of effective nuisance parameters, and the JES uncertainty benefits from the introduction of a pre-recommendation. These uncertainties directly affect the high-level kinematic variables used as input features in the DNN, such as the transverse momenta of the leading and subleading jets and the event-level correlations between them. By providing a more detailed and accurate modelling of these effects, the improved uncertainties reduce unrealistic variations in the input features, which in turn leads to a smaller propagated impact on the DNN classification and the measured signal strength.

Table 5.1: Category-wise impact of systematic uncertainties on the fitted signal strength. Systematic uncertainties of this analysis are compared with the impacts in the previous measurement, taken from [5].

Systematic	Previous measurement: $\frac{\Delta\mu}{\mu}$[%]	Current measurement $\frac{\Delta\mu}{\mu}$[%]
s-channel modelling	$+18/-8$	$+2/-2$
$t\bar{t}$ shape modelling	$+18/-15$	$+6/-5$
Jet Energy Resolution	$+18/-12$	$+11/-9$
Jet Energy Scale	$+18/-13$	$+5/-4$
Jet Vertex Tagger	–	$+1/-1$
MC statistics	$+13/-11$	$+1/-1$
Flavor Tagging	$+12/-10$	$+4/-4$
Luminosity	$+4/-3$	$+1/-1$
Pile-up Reweighting	$+5/-3$	$+4/-3$
Electron	–	$+1/-1$
Muon	–	$+1/-1$
Missing Transverse Momentum	$+1/-1$	$+5/-4$
Background Normalisation	–	$+20/-13$
Systematic uncertainties	$+42/-34$	$+21/-19$
Statistical uncertainties	$+8/-8$	$+12/-6$
Total	$+42/-35$	$+25/-20$

6 Summary and Outlook

A study of the impact of systematic uncertainties on the signal strength $\mu_{\text{s-chan.}}$ of the single top quark s-channel process was performed, as previous measurements were limited by these uncertainties. Monte Carlo simulations corresponding to the Run2 dataset, collected between 2015 - 2018 at $\sqrt{s} = 13\,\text{TeV}$ with the ATLAS detector, were used. Only the leptonic decay mode of the W-boson from the top quark decay was considered, resulting in a signal signature consisting of exactly one charged lepton, the corresponding neutrino inferred from the missing transverse momentum $E_{\text{T}}^{\text{miss}}$, and two b-tagged jets. As the statistical method, a binned profile likelihood fit was performed on an Asimov dataset using a single signal region. The output of a deep neural network was employed as the discriminant variable. The fitted singal strength was found to be $\mu_{\text{s-chan.}} = 1^{+0.25}_{-0.20}$. The systematic uncertainties with the largest impact on the signal strength were discussed. The dominant contributions originate from PS and hadronisation modelling of the single top quark s-channel signal process, jet energy resolution uncertainties at detector level, background modelling uncertainties of the dominant $t\bar{t}$ background, and uncertainties related to pile-up reweighting. Compared to the MEM discriminant used in the previous analysis, the use of the DNN output as discriminant significantly reduces the overall impact of systematic uncertainties on the extracted signal strength.

The following elements represent next steps for future analyses: Adding the remaining uncertainties, especially the PDF uncertainties. These can affect the DNN classification through their impact on the high-level kinematic variables used as input features, especially in regions of high momentum transfer. Furthermore the inclusion of orthogonal control regions rich in background events, to enable a more data driven constraint of modelling and normalisation uncertainties of the background processes. This approach enables the background normalisation factors to be treated as free parameters in the fit and constrained by data rather than relying solely on theoretical cross-section uncertainties. Additionally, the use of a more stringent b-tagging working point can reduce mistag contributions and improve the purity of the events classified as signal. Finally, performing a fit to data allows for a validation of the analysis strategy and demonstrates the improved discriminating power of the DNN output when used as the discriminant variable.

A Appendix

Hier könnte ein Anhang stehen, falls Sie z. B. Code, Konstruktionszeichnungen oder Ähnliches mit in die Arbeit bringen wollen. Im Normalfall stehen jedoch alle Ihre Resultate im Hauptteil der Bachelorarbeit und ein Anhang ist überflüssig.

Bibliography

[1] F. Abe et al. “Observation of Top Quark Production in $\overline{p}p$ Collisions with the Collider Detector at Fermilab.” In: *Phys. Rev. Lett.* 74 (14 Apr. 1995), pp. 2626–2631. DOI: 10.1103/PhysRevLett.74.2626. URL: https://link.aps.org/doi/10.1103/PhysRevLett.74.2626.

[2] Riccardo Maria Bianchi and ATLAS Collaboration. “ATLAS experiment schematic or layout illustration.” General Photo. 2022. URL: https://cds.cern.ch/record/2837191.

[3] S. Chatrchyan et al. “Observation of a new boson at a mass of 125 GeV with the CMS experiment at the LHC.” In: *Physics Letters B* 716.1 (2012), pp. 30–61. ISSN: 0370-2693. DOI: https://doi.org/10.1016/j.physletb.2012.08.021. URL: https://www.sciencedirect.com/science/article/pii/S0370269312008581.

[4] ATLAS Collaboration. “Direct top-quark decay width measurement in the $t\bar{t}$ lepton+jets channel at $\sqrt{s} = 8$ TeV with the ATLAS experiment.” In: *The European Physical Journal C* 78.2 (Feb. 2018). ISSN: 1434-6052. DOI: 10.1140/epjc/s10052-018-5595-5. URL: http://dx.doi.org/10.1140/epjc/s10052-018-5595-5.

[5] ATLAS Collaboration. “Measurement of single top-quark production in the s-channel in proton–proton collisions at

$$\sqrt{s}$$

= 13 TeV with the ATLAS detector.” In: *Journal of High Energy Physics* 2023.6 (2023). ISSN: 1029-8479. DOI: 10.1007/jhep06(2023)191. URL: http://dx.doi.org/10.1007/JHEP06(2023)191.

[6] ATLAS Collaboration. “Measurement of the top quark mass with the ATLAS detector using <mml:math xmlns:mml=”http://www.w3.org/1998/Math/MathML” altimg=”si1.svg”> <mml:mi>t</mml:mi> <mml:mover accent=”true”> <mml:mrow> <mml:mi>t</mml:mi> </mml:mrow> <mml:mrow> <mml:mo stretchy=”false”>¯</mml:mo> </mml:mrow> </mml:mover> </mml:math> events with a high transverse momentum top quark.” In: *Physics Letters B* 867 (Aug. 2025). ISSN: 0370-2693. DOI: 10.1016/j.physletb.2025.139608. URL: http://dx.doi.org/10.1016/j.physletb.2025.139608.

[7] ATLAS Collaboration. "Observation of a new particle in the search for the Standard Model Higgs boson with the ATLAS detector at the LHC." In: *Physics Letters B* 716.1 (2012), pp. 1–29. ISSN: 0370-2693. DOI: https://doi.org/10.1016/j.physletb.2012.08.020. URL: https://www.sciencedirect.com/science/article/pii/S037026931200857X.

[8] DØCollaboration. "Observation of the Top Quark." In: *Phys. Rev. Lett.* 74 (14 Apr. 1995), pp. 2632–2637. DOI: 10.1103/PhysRevLett.74.2632. URL: https://link.aps.org/doi/10.1103/PhysRevLett.74.2632.

[9] Niklas Düser. *Search for single top quark production at ATLAS using Deep Neural Networks and Graph Neural Networks.* Master's Thesis. Sept. 2025.

[10] A. Hayrapetyan et al. "Combination of Measurements of the Top Quark Mass from Data Collected by the ATLAS and CMS Experiments at <mml:math xmlns:mml="http://www.w3.org/1998/Math/MathML" display="inline"><mml:msqrt><mml:mi>s</mml:mi></mml:msqrt></mml:math> = 7 and 8 TeV." In: *Physical Review Letters* 132.26 (June 2024). ISSN: 1079-7114. DOI: 10.1103/physrevlett.132.261902. URL: http://dx.doi.org/10.1103/PhysRevLett.132.261902.

[11] Makoto Kobayashi and Toshihide Maskawa. "CP-Violation in the Renormalizable Theory of Weak Interaction." In: *Progress of Theoretical Physics* 49.2 (Feb. 1973), pp. 652–657. DOI: 10.1143/PTP.49.652. eprint: https://academic.oup.com/ptp/article-pdf/49/2/652/5257692/49-2-652.pdf. URL: https://doi.org/10.1143/PTP.49.652.

[12] S. Navas et al. "Review of Particle Physics." In: *Phys. Rev. D* 110 (3 Aug. 2024), p. 030001. DOI: 10.1103/PhysRevD.110.030001. URL: https://link.aps.org/doi/10.1103/PhysRevD.110.030001.

[13] Andrés Pinto et al. *Uncertainty components in profile likelihood fits.* 2024. arXiv: 2307.04007 [physics.data-an]. URL: https://arxiv.org/abs/2307.04007.

[14] Pienpen Seema et al. *Search for single top-quark production in the s-channel in proton-proton collisions at* $\sqrt{s}=13$ *TeV.* Tech. rep. Geneva: CERN, 2010. URL: https://cds.cern.ch/record/2706904.

[15] Nicola Serra. *Standard Model.* 2025. URL: https://www.physik.uzh.ch/groups/serra/StandardModel.html.

[16] *Studies on the improvement of the matching uncertainty definition in top-quark processes simulated with Powheg+Pythia 8.* Tech. rep. All figures including auxiliary figures are available at https://atlas.web.cern.ch/Atlas/GROUPS/PHYSICS/PUBNOTES/ATL-PHYS-PUB-2023-029. Geneva: CERN, 2023. URL: https://cds.cern.ch/record/2872787.

Eidesstattliche Versicherung

(Affidavit)

Name, Vorname
(surname, first name)

Matrikelnummer
(student ID number)

☐ Bachelorarbeit
(Bachelor's thesis)

☐ Masterarbeit
(Master's thesis)

Titel
(Title)

Ich versichere hiermit an Eides statt, dass ich die vorliegende Abschlussarbeit mit dem oben genannten Titel selbstständig und ohne unzulässige fremde Hilfe erbracht habe. Ich habe keine anderen als die angegebenen Quellen und Hilfsmittel benutzt sowie wörtliche und sinngemäße Zitate kenntlich gemacht. Die Arbeit hat in gleicher oder ähnlicher Form noch keiner Prüfungsbehörde vorgelegen.

I declare in lieu of oath that I have completed the present thesis with the above-mentioned title independently and without any unauthorized assistance. I have not used any other sources or aids than the ones listed and have documented quotations and paraphrases as such. The thesis in its current or similar version has not been submitted to an auditing institution before.

Ort, Datum
(place, date)

Unterschrift
(signature)

Belehrung:
Wer vorsätzlich gegen eine die Täuschung über Prüfungsleistungen betreffende Regelung einer Hochschulprüfungsordnung verstößt, handelt ordnungswidrig. Die Ordnungswidrigkeit kann mit einer Geldbuße von bis zu 50.000,00 € geahndet werden. Zuständige Verwaltungsbehörde für die Verfolgung und Ahndung von Ordnungswidrigkeiten ist der Kanzler/die Kanzlerin der Technischen Universität Dortmund. Im Falle eines mehrfachen oder sonstigen schwerwiegenden Täuschungsversuches kann der Prüfling zudem exmatrikuliert werden. (§ 63 Abs. 5 Hochschulgesetz - HG -).

Die Abgabe einer falschen Versicherung an Eides statt wird mit Freiheitsstrafe bis zu 3 Jahren oder mit Geldstrafe bestraft.

Die Technische Universität Dortmund wird ggf. elektronische Vergleichswerkzeuge (wie z.B. die Software „turnitin") zur Überprüfung von Ordnungswidrigkeiten in Prüfungsverfahren nutzen.

Die oben stehende Belehrung habe ich zur Kenntnis genommen:

Official notification:
Any person who intentionally breaches any regulation of university examination regulations relating to deception in examination performance is acting improperly. This offense can be punished with a fine of up to EUR 50,000.00. The competent administrative authority for the pursuit and prosecution of offenses of this type is the Chancellor of TU Dortmund University. In the case of multiple or other serious attempts at deception, the examinee can also be unenrolled, Section 63 (5) North Rhine-Westphalia Higher Education Act (*Hochschulgesetz, HG*).

The submission of a false affidavit will be punished with a prison sentence of up to three years or a fine.

As may be necessary, TU Dortmund University will make use of electronic plagiarism-prevention tools (e.g. the "turnitin" service) in order to monitor violations during the examination procedures.

I have taken note of the above official notification:*

Ort, Datum
(place, date)

Unterschrift
(signature)

***Please be aware that solely the German version of the affidavit ("Eidesstattliche Versicherung") for the Bachelor's/ Master's thesis is the official and legally binding version.**